

# Compact Magnetic Antennas for Directional Excitation of Surface Plasmons

Yongmin Liu,<sup>†,§</sup> Stefano Palomba,<sup>†,§</sup> Yongshik Park,<sup>†</sup> Thomas Zentgraf,<sup>†</sup> Xiaobo Yin,<sup>†,‡</sup> and Xiang Zhang<sup>\*,†,‡</sup>

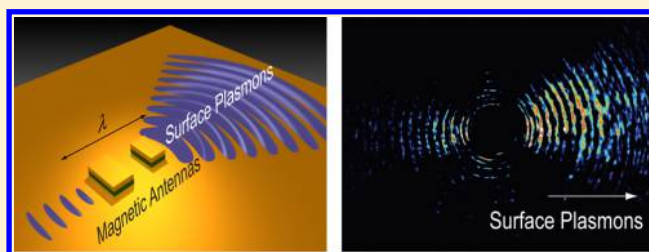
<sup>†</sup>NSF Nanoscale Science and Engineering Center (NSEC), 3112 Etcheverry Hall, University of California, Berkeley, California 94720, United States

<sup>‡</sup>Materials Science Division, Lawrence Berkeley National Laboratory, 1 Cyclotron Road, Berkeley, California 94720, United States

## S Supporting Information

**ABSTRACT:** Plasmonics is considered as one of the most promising candidates for implementing the next generation of ultrafast and ultracompact photonic circuits. Considerable effort has been made to scale down individual plasmonic components into the nanometer regime. However, a compact plasmonic source that can efficiently generate surface plasmon polaritons (SPPs) and deliver SPPs to the region of interest is yet to be realized. Here, bridging the optical antenna theory and the recently developed concept of metamaterials, we demonstrate a subwavelength, highly efficient plasmonic source for directional generation of SPPs. The designed device consists of two nanomagnetic resonators with detuned resonant frequencies. At the operating wavelength, incident photons can be efficiently channeled into SPP waves modulated by the electric field polarization. By tailoring the relative phase at resonance and the separation between the two nanoresonators, SPPs can be steered to predominantly propagate along one specific direction. This novel magnetic nanoantenna paves a new way to manipulate photons in the near-field, and also could be useful for SPP-based nonlinear applications, active modulations, and wireless optical communications.

**KEYWORDS:** Plasmonics, nanoantennas, metamaterials, resonators



For over 50 years, photonic structures and devices have produced remarkable outcomes in telecommunications, information processing, and biomedical sensing. The miniaturization of photonic devices may potentially enable chip-scale processors and communication systems with low power consumption, ultrahigh-resolution imaging and lithography, as well as new sensors with unprecedented sensitivity and specificity. As an emerging branch in nanophotonics, plasmonics has achieved substantial advancements during the past decade, thanks to the unique properties of subwavelength optical confinement and significant field enhancement of SPPs in metallic nanostructures. The vibrant and interactive research of plasmonics has resulted in exciting applications in multiple disciplines, ranging from nearfield microscopy and spectroscopy, biomedical sensing, photovoltaics, to integrated optical devices.<sup>1–3</sup> In particular, various plasmonic optical components, including lenses,<sup>4</sup> reflectors,<sup>5</sup> waveguides,<sup>6</sup> demultiplexers,<sup>7</sup> and modulators,<sup>8</sup> have been reported, demonstrating the potential capabilities of plasmonics to shrink the photonic circuits below the diffraction limit.

As one of the key elements for the future implementation of plasmonic devices, SPP sources, which are either optically<sup>9–17</sup> or electrically driven,<sup>18–20</sup> have attracted considerable attention. The conventional optical scheme to efficiently convert free-space light into SPP modes utilizes prisms and gratings.<sup>21</sup> However, these “bulky” optical configurations are not ideal for

high-density integration and fast modulation. In order to overcome this limitation, nanostructures on the metal surface, such as a single subwavelength slit<sup>9–11</sup> or an aperture<sup>12–14</sup> that is isolated or dressed by shallow corrugations, have been used to launch SPPs. Nevertheless, these configurations present the disadvantage that only a small fraction of the impinging light is coupled into SPP modes. Moreover, light orthogonally incident on an asymmetric structure can generate surface waves propagating only along one direction due to the interference of plasmon waves.<sup>15–17</sup>

In this letter, we theoretically conceive and experimentally demonstrate a novel resonant optical antenna that serves as an efficient and directional plasmonic source. As the counterpart of radio wave and microwave antennas, optical antennas have emerged as a new scheme to manipulate the transmission and reception of optical fields at the nanoscale.<sup>22,23</sup> Many intriguing phenomena and applications, such as controllable or enhanced light emission,<sup>24,25</sup> compact photodetectors,<sup>26,27</sup> high-resolution microscopy<sup>28,29</sup> and low-power optical trapping,<sup>30</sup> have been realized in the context of optical antennas. In particular, the emission of a quantum emitter into free space is

Received: June 23, 2012

Revised: July 20, 2012

Published: July 30, 2012

considerably modified when the emitter is located close to an optical antenna.<sup>31–34</sup>

Applying the optical antenna theory, we utilize paired metamaterial structures to efficiently excite SPPs and steer these evanescent waves to propagate predominantly along one specific and predetermined direction. Figure 1 schematically

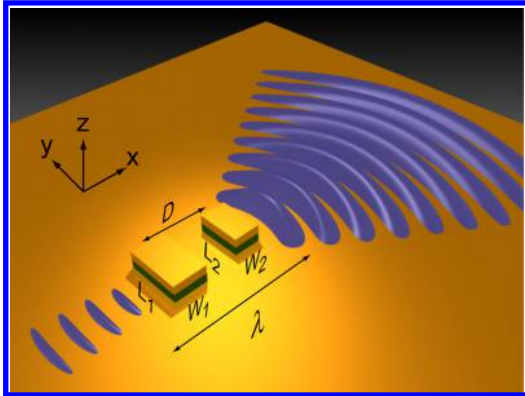


**Figure 1.** Schematic of the compact magnetic antenna that can generate directional SPPs. The antenna consists of two magnetic resonators with different geometries. Each magnetic resonator is made of a metallic nanodisk that is separated from a metal substrate by a dielectric layer.

shows the configuration of the device. It consists of two building blocks, each of which is a metallic nanodisk on top of a metal surface sandwiched with a dielectric layer. Because of the coupling with its mirror image in the metal substrate, the metallic nanodisk supports strong magnetic resonance,<sup>35,36</sup> which has been widely studied in the field of metamaterials.<sup>37–39</sup> The magnetic resonance frequency can be readily controlled by the geometry of the disk, the thickness of the dielectric layer, and the material dielectric function, offering an extra degree of freedom in the design compared with

conventional optical antennas. At the resonance, the nano-magnetic resonator strongly interacts with light, and when the resonator reradiates energy, part of the light will be coupled into SPP modes. The excited SPPs generated by the asymmetric resonators constructively or destructively interfere, depending on the working frequency and the distance between the two resonators. As a result, the propagation of SPPs can be directional. To the best of our knowledge, it is the first demonstration of directional excitation of SPPs based on metamaterial structures. As demonstrated in the following, the dimension of the device is smaller than the wavelength of light in all three dimensions compared with early work,<sup>15–17</sup> and the generation efficiency of SPPs is several times higher than previous designs thanks to the strong resonance nature of the magnetic metamaterial structure. Furthermore, we expect that our approach of using magnetic resonators (magnetic dipoles) can also be applied to control free-space propagating waves, in contrast to conventional optical antennas based on assembly of metallic nanostructures (electric dipoles).

We first perform numerical simulations of individual magnetic resonators to better understand the underlying mechanism (Commercial software CST Microwave Studio and COMSOL Multiphysics are used for the simulations). The width ( $W_1$ ) and the length ( $L_1$ ) of the large resonator are 315 and 185 nm, respectively, and the corresponding values ( $W_2$  and  $L_2$ ) for the small resonator are 250 and 150 nm, respectively. Both the metallic disk and the dielectric spacing layer are 40 nm thick. Low-index dielectric  $\text{MgF}_2$  (refractive index  $n = 1.35$ ) is used as the spacing layer, and gold is chosen for the metallic disk and the substrate. The permittivity of gold ( $\epsilon_m(\omega)$ ) is described as the Drude model by fitting the experimental data from the literature.<sup>40</sup> The excitation plane wave normally impinges on the resonator, and the magnetic field polarizes along the  $y$ -axis. Figure 2a depicts the distribution of the magnetic field (color map) and the displacement current (black arrows) at resonance. The displacement current clearly forms a loop, implying a strong

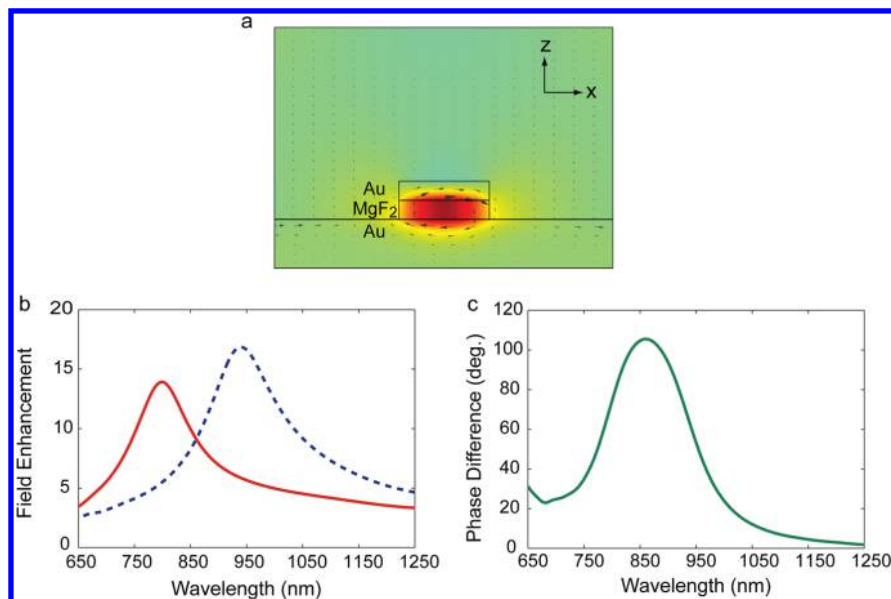


**Figure 2.** Magnetic resonance of the resonator. (a) The color map shows the magnetic field ( $H_y$ ) distribution of the resonator, while the black arrows represent the electric displacement current. (b) The enhancement of the local magnetic field at the center of the two resonators. The blue dashed curve corresponds to the spectrum of the resonator with length  $L_1 = 315$  nm and width  $W_1 = 185$  nm, and the red curve is for a smaller resonator with  $L_2 = 250$  nm and  $W_2 = 150$  nm. (c) The relative phase difference of the two resonators.

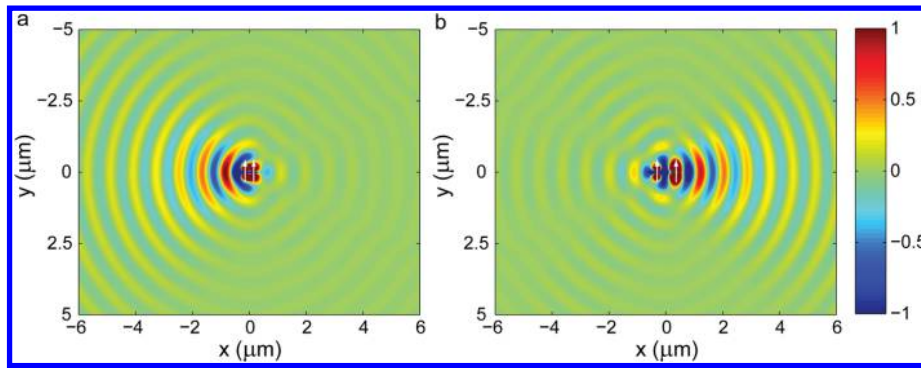


**Figure 3.** The electric field distribution of SPPs under the magnetic dipole approximation. The distance of the two dipoles is (a) 300 nm and (b) 600 nm, respectively. The phase difference of the two dipoles at a wavelength of 820 nm is taken from Figure 2c.

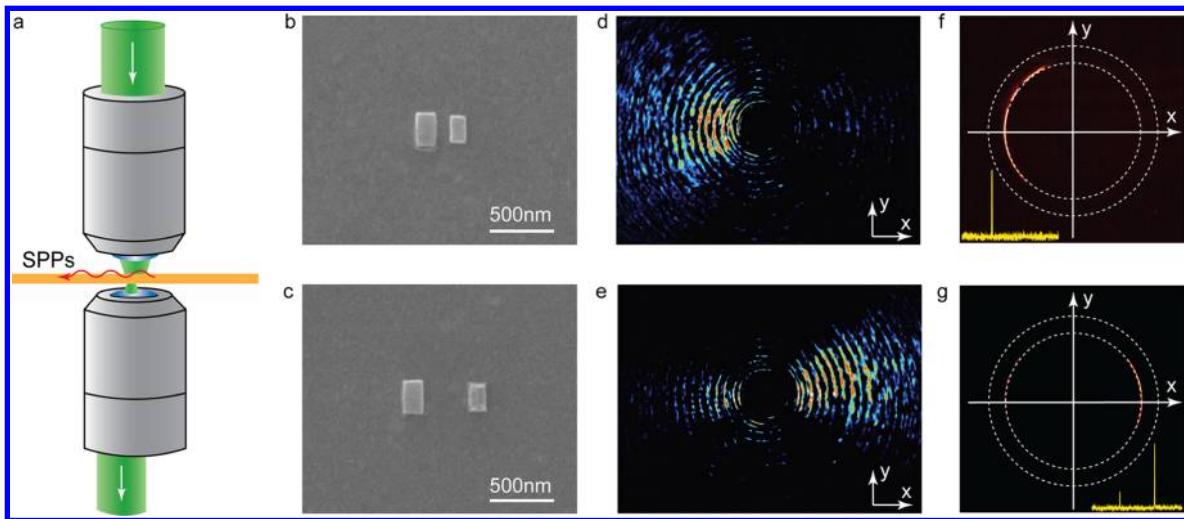


**Figure 4.** Experimental demonstration of the directional excitation of SPPs. (a) Schematic illustration of the experimental setup. (b, c) Scanning electron microscope (SEM) images of the fabricated nanoantenna sample. The distance between the two magnetic resonators is 300 and 600 nm, respectively. (d, e) Leakage radiation microscopy results for nanoantennas (b, c), respectively. The collected phase fronts of the SPPs launched at the air–gold interface are irrefutably directional and are remarkably in agreement with the theoretical simulation shown in Figure 3. (f, g) Respective Fourier plane of the images (d) and (e). The leakage radiation collected by the oil immersion objective clearly confirms the directionality of the SPP waves, which are emitted just above the critical angle (smaller dashed circle), as expected from the evanescent nature of SPPs. The yellow curves in the insets of (f, g) represent the line profile along the *x*-axis of the Fourier plane.

magnetic moment. In Figure 2b, we plot the magnetic field at the center of the MgF<sub>2</sub> layer. The peaks in the spectra indicate the resonance wavelengths. Compared with a larger resonator, a smaller one resonates at relatively shorter wavelength due to the reduced capacitance and inductance of the structure. As expected, there is a relative phase difference between the two resonators, as shown in Figure 2c, which will be used as a key parameter in the design of the magnetic nanoantennas.

The magnetic resonator can be modeled as a magnetic dipole oscillating along the *y*-axis, owing to its subwavelength dimensions. Similar to an electric dipole, the large wave vector components of the magnetic dipole can launch SPPs when the antenna is close to a metal surface. Because the two magnetic resonators oscillate with different phases, the excited surface waves constructively or destructively interfere, resulting in directional propagation of SPPs. In order to confirm our prediction, we numerically calculate the field distribution of SPPs in the *x*–*y* plane, which are excited by two magnetic dipoles with different phases. Under the dipole approximation, the radiated field of SPPs from one magnetic dipole is given by<sup>41</sup>

$$E = -\frac{c\mu_0 k_{sp}^2}{4\pi} \frac{e^{ik_{sp}r}}{r} (\hat{n} \times \vec{m}) \left( 1 - \frac{1}{ik_{sp}r} \right) \quad (1)$$

where  $\vec{m}$  indicates the magnetic dipole,  $\hat{n}$  is the unit vector in the direction of  $\vec{r}$  with respect to the position of the dipole, and  $k_{sp}$  is the wave vector of SPPs given by  $k_{sp} = (2\pi/\lambda)[\epsilon_m(\omega)/(\epsilon_m(\omega) + 1)]^{1/2}$ . Parts a and b of Figure 3 plot the field for two magnetic dipoles with separation distance  $D = 300$  nm and  $D = 600$  nm, respectively. The wavelength  $\lambda$  is 820 nm, and the phase difference of the two magnetic dipoles is taken from Figure 2c. One can clearly see the directional propagation of SPPs for both cases, while propagating in opposite directions. To further confirm our design, we perform three-dimensional full wave simulations considering the realistic geometry of the structure (Supporting Information), in which the field distributions show excellent agreement with the results based on the dipole approximation. We also quantitatively compare the integrated intensity of SPPs in the negative and positive half space of the *x*-axis, which gives a ratio of 10.5:1 and 1:9.7, respectively, as the distance of the two magnetic resonators is 300 and 600 nm.

We employ leakage radiation microscopy and conoscopic detection on single antennas to experimentally demonstrate the directional excitation of SPPs at the air-gold interface.<sup>11,14,42</sup> The experimental setup is schematically illustrated in Figure 4a. Two objectives are confocally aligned and used for the excitation (top) and the detection (bottom) of the SPP wave and its leakage radiation. A pulsed Ti:sapphire laser with 130 fs pulses and 40  $\mu\text{W}$  average power at a wavelength of 820 nm is used as the coherent excitation source. The pump beam is launched through the top objective (40 $\times$ , 0.65 NA) and strongly interacts with the nanoantennas. The excited SPPs at the air-gold interface can radiatively leak through the thin metal film and be collected by the bottom oil immersion objective (100 $\times$ , 1.4 NA). Imaging the Fourier plane of the bottom objective provides the measurement of the refracted angle and the direction of the propagating SPP wave at the air-gold interface. The images at the object plane and the Fourier plane are both taken by standard charge-coupled devices (CCD).

We fabricate the nanoantennas by the standard electron beam lithography technique. Figure 4b and c shows the scanning electron microscope images of the fabricated nanoantennas. We first test and calibrate the detection system by illuminating a grating fabricated on the same substrate used to fabricate the resonant nanoantennas (Supporting Information). In this case, two clear SPP jets can be observed, which symmetrically propagate away from the grating structure along the polarization axis. Imaging the Fourier plane allows the propagation directions of the wavevectors in  $k$ -space to be mapped into the physical space. The two symmetric lobes in the  $k$ -space clearly indicate that the wavevectors of the two launched SPP jets are in opposite directions.

The images of leakage radiation and their conoscopic images at the Fourier plane for single antenna structures are shown in Figure 4d–g. One can notice that the leakage radiation images (Figure 4d and e) exhibit typical fringe patterns, which arise from the interference of the directly transmitted light and the leakage radiation of SPPs. Because of the laser light coherence, such interference fringes provide the phase information of the SPPs propagating along the surface. In the case of a separation of  $D = 300$  nm and electric field polarization along the  $x$ -axis (Figure 4d), we observe that the SPP phase front propagates away from the nanostructures along the  $-x$  direction, which is consistent with the numerical simulation (Figure 3a). The experimental result shown in Figure 4d is after proper normalization to reduce the background noise. In order to normalize the data, we image the structures under the same excitation intensity but with a different electric field polarization (along the  $y$ -axis). In this case, the excited SPPs are negligible, since the resonators are off resonance. The corresponding radiation pattern in the  $k$ -space for  $D = 300$  nm is represented by the Fourier plane image in Figure 4f. The outer white-dashed circle in Figure 4f represents the objective back-aperture borderline, whereas the inner one represents the angle at which light is totally internally refracted (TIR). The leakage radiation from the propagating SPP wave generates a radiation pattern constituted by a dominant lobe at higher emitted angles than the TIR ring. The presence of a single lobe is a clear indication of the directionality of the SPP phase front. The lobe is located at a slightly larger axial location than the position of the TIR ring at the Fourier plane, confirming the observed signals are indeed SPPs at the air-gold interface. The inset in Figure 4f represents the line-cut along the horizontal  $x$ -axis. The ratio of

the peak intensities between the backward propagating SPPs (along  $-x$  axis) and the forward propagating SPPs (along  $+x$  axis) is about 2.69, clearly showing the good directionality of the SPPs. Figure 4e shows that the phase front of the SPPs dramatically changes direction for the interparticle separation equal to 600 nm. In this case, the SPPs propagate along the  $+x$  direction. The leakage radiation imaged at the Fourier plane (Figure 4g) shows a lobe in diametrically opposite direction, compared to the case of a smaller interparticle separation ( $D = 300$  nm). From Figure 4g, we can determine that the ratio between SPP propagating along the forward and backward direction is about 1.66.

It has to be noticed that the radiation angle of SPPs appears large, since we only have two magnetic resonators in the current design. In principle, enhanced directionality (i.e., a narrower radiation angle) can be realized by incorporating more resonators with carefully designed geometries, which function individually as the reflector, feed, and director similar to the Yagi-Uda antenna. Furthermore, when normalized to the energy per unit area, a magnetic resonator converts light illuminating an area of 1.35 times larger than its physical size into SPPs. That is, the excitation efficiency can be more accurately estimated to be about 135% (red circles in Figure 5).

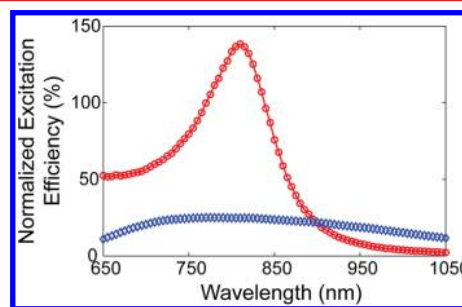


**Figure 5.** The spectral response of the normalized excitation efficiency of SPPs for a magnetic resonator (red circles) and a nano aperture (blue diamonds). The length and width of the magnetic resonator are 250 and 150 nm, respectively. The aperture is milled through a 50 nm gold film but with the same physical dimension.

Such a high efficiency can be attributed to the strong resonance nature of magnetic resonators and thus a large scattering cross section. For comparison, we simulate the normalized excitation efficiency for an aperture (blue diamonds in Figure 5) with the same physical dimension (250 nm  $\times$  150 nm) that is milled through a 50 nm gold film. The excitation efficiency of SPPs shows a broader spectral response with the maximum efficiency of about 25% centered at 780 nm wavelength. The calculated efficiency is consistent with previous work considering different aperture geometries,<sup>14</sup> although here we did not purposely optimize the aperture size. Therefore, the efficiency of our magnetic antennas is at least 5 times larger than that of single apertures, and also 3 times larger than the single slits case,<sup>10,11</sup> which are both plasmon sources using scatters (electric dipoles). It is interesting to further compare the excitation efficiency of electric and magnetic antennas with different designs, which we will present somewhere else in the future.

In conclusion, we have theoretically and experimentally demonstrated a compact nanoantenna constituted by a pair of magnetic resonators, which can efficiently generate directional SPP waves. Leakage radiation microscopy on single magnetic antennas clearly demonstrates the highly directional propaga-

tion of the SPPs at the air–gold interface, in very good agreement with the theoretical and numerical analysis. The efficient generation of SPPs in the magnetic nanoantennas is superior to previous work based on single slits or single apertures, thanks to the strong resonance nature of magnetic resonators. The device is subwavelength in all three dimensions, which will be a fundamental building block for the next generation of integrated plasmonic circuits. The metal–insulator–metal geometry in our design may facilitate the further development of directional plasmon sources with electrical pumping, when semiconductor or organic materials are used in the spacing layer.<sup>18,19</sup> The device can perform as a SPP generator, point-to-point wireless interconnect, or planar biochemical sensor. Finally, by incorporating emitters into the magnetic antenna, we may enhance transition rates, increasing the emission efficiency and the coupling between emitters and surface plasmons for potential quantum optical applications.

## ■ ASSOCIATED CONTENT

### 📄 Supporting Information

The three-dimensional full wave simulation of the realistic antenna structure, as well as the optical measurements using a grating to excite surface plasmons for system calibration purposes. This material is available free of charge via the Internet at <http://pubs.acs.org>.

## ■ AUTHOR INFORMATION

### Corresponding Author

\*E-mail: [xiang@berkeley.edu](mailto:xiang@berkeley.edu).

### Author Contributions

<sup>§</sup>These authors contributed equally to this work.

### Notes

The authors declare no competing financial interest.

## ■ ACKNOWLEDGMENTS

The authors acknowledge funding support from the US Army Research Office (MURI program W911NF-09-1-0539) and the US National Science Foundation (NSF Nanoscale Science and Engineering Center CMMI-0751621).

## ■ REFERENCES

- (1) Barnes, W. L.; Dereux, A.; Ebbesen, T. W. Surface plasmon subwavelength optics. *Nature* **2003**, *424*, 824–830.
- (2) Halas, N. J. Plasmonics: an emerging field fostered by Nano Letters. *Nano Lett.* **2010**, *10*, 3816–3822.
- (3) Schuller, J. A.; Barnard, E. S.; Cai, W. S.; Jun, Y. C.; White, J. S.; Brongersma, M. L. Plasmonics for extreme light concentration and manipulation. *Nat. Mater.* **2010**, *9*, 193–204.
- (4) Ditlbacher, H.; Krenn, J. R.; Schider, G.; Leitner, A.; Aussenegg, F. R. Two-dimensional optics with surface plasmon polaritons. *Appl. Phys. Lett.* **2002**, *81*, 1762–1764.
- (5) Weeber, J.-C.; Lacroute, Y.; Dereux, A.; Devaux, E.; Ebbesen, T.; Girard, C.; González, M. U.; Baudrion, A.-L. Near-field characterization of Bragg mirrors engraved in surface plasmon waveguides. *Phys. Rev. B* **2004**, *70*, 235406.
- (6) Bozhevolnyi, S. I.; Volkov, V. S.; Devaux, E.; Laluet, J. Y.; Ebbesen, T. W. Channel plasmon subwavelength waveguide components including interferometers and ring resonators. *Nature* **2006**, *440*, 508–511.
- (7) Drezet, A.; Koller, D.; Hohenau, A.; Leitner, A.; Aussenegg, F. R.; Krenn, J. R. Plasmonic Crystal Demultiplexer and Multiplexers. *Nano Lett.* **2007**, *7*, 1697–1700.
- (8) Dionne, J. A.; Diest, K.; Sweatlock, L. A.; Atwater, H. A. PlasMOStor: a metal–oxide–Si field effect plasmonic modulator. *Nano Lett.* **2009**, *9*, 897–902.
- (9) Lezec, H. J.; Degiron, A.; Devaux, E.; Linke, R. A.; Martin-Moreno, L.; Garcia-Vidal, F. J.; Ebbesen, T. W. Beaming light from a subwavelength aperture. *Science* **2002**, *297*, 820–822.
- (10) Lalanne, P.; Hugonin, J. P.; Rodier, J. C. Theory of surface plasmon generation at nanoslit apertures. *Phys. Rev. Lett.* **2005**, *95*, 263902.
- (11) Laluet, J.-Y.; Drezet, A.; Genet, C.; Ebbesen, T. W. Generation of surface plasmons at single subwavelength slits: from slit to ridge plasmon. *New J. Phys.* **2008**, *10*, 105014.
- (12) Sönnichsen, C.; Duch, A. C.; Steininger, G.; Koch, M.; von Plessen, G.; Feldmann, J. Launching surface plasmons into nanoholes in metal films. *Appl. Phys. Lett.* **2000**, *76*, 140–142.
- (13) Yin, L.; Vlasko-Vlasov, V. K.; Rydh, A.; Pearson, J.; Welp, U.; Chang, S.-H.; Gray, S. K.; Schatz, G. C.; Brown, D. B.; Kimball, C. W. Surface plasmons at single nanoholes in Au films. *Appl. Phys. Lett.* **2004**, *85*, 467–469.
- (14) Baudrion, A.-L.; et al. Coupling efficiency of light to surface plasmon polariton for single subwavelength holes in a gold film. *Opt. Express* **2008**, *16*, 3420–3429.
- (15) López-Tejeda, F.; et al. Efficient unidirectional nanoslit couplers for surface plasmons. *Nat. Phys.* **2007**, *3*, 324–328.
- (16) Chen, J. J.; Li, Z.; Yue, S.; Gong, Q. H. Efficient unidirectional generation of surface plasmon polaritons with asymmetric single-nanoslit. *Appl. Phys. Lett.* **2010**, *97*, 041113.
- (17) Liu, J. S. Q.; Pala, R. A.; Afshinmanesh, F.; Cai, W. S.; Brongersma, M. L. A submicron plasmonic dichroic splitter. *Nat. Commun.* **2011**, *2*, 525.
- (18) Koller, D. M.; Hohenau, A.; Ditlbacher, H.; Galler, N.; Aussenegg, F. R.; Leitner, A.; Krenn, J. R.; Eder, S.; Sax, S.; List, E. J. W. Surface plasmon coupled electroluminescent emission. *Appl. Phys. Lett.* **2008**, *92*, 103304.
- (19) Walters, R. J.; van Loon, R. V. A.; Brunets, I.; Schmitz, J.; Polman, A. A silicon-based electrical source of surface plasmon polaritons. *Nat. Mater.* **2009**, *9*, 21–25.
- (20) Bharadwaj, P.; Bouhelier, A.; Novotny, L. Electrical excitation of surface plasmons. *Phys. Rev. Lett.* **2011**, *106*, 226802.
- (21) Raether, H. *Surface Plasmons: On Smooth and Rough Surfaces and on Gratings*; Springer: Berlin, 1988.
- (22) Novotny, L.; van Hulst, N. Antennas for light. *Nat. Photonics* **2011**, *5*, 83–90.
- (23) Giannini, V.; Fernandez-Dominguez, A. I.; Heck, S. C.; Maier, S. A. Plasmonic nanoantennas: Fundamentals and their use in controlling the radiative properties of nanoemitters. *Chem. Rev.* **2011**, *111*, 3888–3912.
- (24) Tamini, T. H.; Stefani, F. D.; Segerink, F. B.; van Hulst, N. F. Optical antennas direct single-molecule emission. *Nat. Photonics* **2008**, *2*, 234–237.
- (25) Kinkhabwala, A.; Yu, Z. F.; Fan, S. H.; Avlasevich, Y.; Mullen, K.; Moerner, W. E. Large single-molecule fluorescence enhancements produced by a bowtie nanoantenna. *Nat. Photonics* **2009**, *3*, 654–657.
- (26) Tang, L.; et al. Nanometre-scale germanium photodetector enhanced by a near-infrared dipole antenna. *Nat. Photonics* **2008**, *2*, 226–229.
- (27) Knight, M. W.; Sobhani, H.; Nordlander, P.; Halas, N. J. Photodetection with active optical antennas. *Science* **2011**, *332*, 702–704.
- (28) Sanchez, E. J.; Novotny, L.; Xie, X. S. Near-field fluorescence microscopy based on two-photon excitation with metal tips. *Phys. Rev. Lett.* **1999**, *82*, 4014–4017.
- (29) Palomba, S.; Novotny, L. Near-field imaging with a localized nonlinear light source. *Nano Lett.* **2009**, *9*, 3801–4804.
- (30) Juan, M. L.; Righini, M.; Quidant, R. Plasmon nano-optical tweezers. *Nat. Photonics* **2011**, *5*, 349–356.
- (31) Li, J. J.; Salandrino, A.; Engheta, N. Shaping light beams in the nanometer scale: A Yagi-Uda nanoantenna in the optical domain. *Phys. Rev. B* **2007**, *76*, 245403.

- (32) Kosako, T.; Kadoya, Y.; Hofmann, H. F. Directional control of light by a nano-optical Yagi–Uda antenna. *Nat. Photonics* **2010**, *4*, 312–315.
- (33) Curto, A. G.; Volpe, G.; Taminiau, T. H.; Kreuzer, M. P.; Quidant, R.; van Hulst, N. F. Unidirectional emission of a quantum dot coupled to a nanoantenna. *Science* **2010**, *329*, 930–933.
- (34) Dregely, D.; Taubert, R.; Dorfmueller, J.; Vogelgesang, R.; Kern, K.; Giessen, H. 3D optical Yagi–Uda nanoantenna array. *Nat. Commun.* **2011**, *2*, 267.
- (35) Zhang, S.; Fan, W. J.; Minhas, B. K.; Frauenglass, A.; Malloy, K. J.; Bruech, S. R. J. Midinfrared resonant magnetic nanostructures exhibiting a negative permeability. *Phys. Rev. Lett.* **2005**, *94*, 037402.
- (36) Liu, N.; Mesch, M.; Weiss, T.; Hentschel, M.; Giessen, H. Infrared perfect absorber and its application as plasmonic sensor. *Nano Lett.* **2010**, *10*, 2342–2348.
- (37) Smith, D. R.; Pendry, J. B.; Wiltshire, M. C. K. Metamaterials and negative refractive index. *Science* **2004**, *305*, 788–792.
- (38) Soukoulis, C. M.; Linden, S.; Wegener, M. Negative refractive index at optical wavelengths. *Science* **2007**, *315*, 47–49.
- (39) Liu, Y. M.; Zhang, X. Metamaterials: a new frontier of science and technology. *Chem. Soc. Rev.* **2011**, *40*, 2094–2107.
- (40) Johnson, P. B.; Christy, R. W. Optical constants of the noble metals. *Phys. Rev. B* **1972**, *6*, 4370–4379.
- (41) Jackson, J. D. *Classical Electromagnetics*, 3rd ed.; John Wiley & Sons: New York, 1999.
- (42) Zentgraf, T.; Liu, Y. M.; Mikkelsen, M. H.; Valetine, J.; Zhang, X. Plasmonic Luneburg and Eaton lenses. *Nat. Nanotechnol.* **2011**, *6*, 151–155.